ELSEVIER

Earth and Planetary Science Letters 186 (2001) 269–281

EPSL

www.elsevier.com/locate/epsl

Modulation of erosion on steep granitic slopes by boulder armoring, as revealed by cosmogenic ^{26}Al and ^{10}Be

Darryl E. Granger [a,*], Clifford S. Riebe [b], James W. Kirchner [b], Robert C. Finkel [c]

[a] *PRIME Laboratory and Department of Earth and Atmospheric Sciences, Purdue University, West Lafayette, IN 47907-1397, USA*
[b] *Department of Earth and Planetary Science, University of California, Berkeley, CA 94720-4767, USA*
[c] *Center for Accelerator Mass Spectrometry, Lawrence Livermore National Laboratory, Livermore, CA 94551-9900, USA*

Received 25 September 2000; received in revised form 4 January 2001; accepted 5 January 2001

Abstract

Cosmogenic ^{26}Al and ^{10}Be in quartz from boulders, bedrock and sandy sediment from 21 small watersheds in the Diamond Mountains batholith, CA, USA, and two small watersheds from the nearby Fort Sage Mountains confirm that exposed granitic bedrock and boulders erode more slowly than the catchments in which they are found. Exposed bedrock and boulders are more abundant on steep slopes and may play an important role in regulating mountain erosion rates. Rapid transport of fine sediment on steep slopes exhumes resistant corestones which accumulate on the surface. The resulting boulder lag apparently shields the underlying soil and bedrock from erosion, even when the bedrock is deeply weathered and friable. Where steep slopes have an abundant boulder lag, they erode as slowly as gentler slopes nearby. In contrast, steep slopes lacking a boulder lag erode much more quickly than gentle slopes. Boulder armoring can modulate hillslope erosion such that erosion rates of summits, steep mountain flanks, and gentle footslopes are indistinguishable, thus permitting local relief and steep mountain slopes to persist for long periods of time.

Keywords: cosmogenic elements; erosion; granitic rocks; weathering; boulders

1. Introduction

Soil cover has long been recognized as important for chemical weathering of bedrock (e.g. [1]). Exposed bedrock remains dry most of the time and weathers slowly, whereas bedrock beneath a soil or regolith cover can remain perennially moist with soil solutions that promote mineral alteration. Feedbacks between regolith thickness and bedrock weathering rate have important implications for hillslope evolution (e.g. [2,3]). For example, Heimsath et al. studied small catchments developed in greenstone melange near San Francisco Bay, CA, USA [4,5], and in granitic rocks in the Bega Valley, Australia [6], and used cosmogenic nuclides to show that the rate of conversion of bedrock to soil depends on soil depth. Bedrock beneath shallow soils on convex noses is rapidly converted to soil, while similar bedrock beneath

* Corresponding author. Fax: +1-765-496-1210; E-mail: dgranger@purdue.edu

0012-821X/01/$ – see front matter
PII: S0012-821X(01)00236-9

deeper soils is more slowly decomposed. Heimsath et al. [4–6] also showed that exposed bedrock in their study catchments erodes far more slowly than similar rock beneath soil cover. Bedrock exposed by chance, then, can remain resistant to erosion while the surrounding landscape lowers around it, leaving the bedrock protruding as an outcrop or a tor. Such differences in the erosion rates of exposed and buried bedrock are at the heart of classic models of tor and bornhardt development in areas of intense subsoil weathering (e.g. [7–10]).

In soil-mantled landscapes where bare rock outcrops are common, differences between the erosion rates of bare and soil-mantled rock may affect hillslope erosion rates and thus help modulate hillslope relief. In most temperate landscapes, however, tors and bornhardts are too scarce to substantially affect hillslope evolution. A notable exception is found in granitic terrain, where tors and bare rock slopes are commonplace. The presence of soil cover is thought to be particularly important in chemical weathering of granite, especially in the granular disintegration that is common in biotite-bearing granitic rocks. Biotite and plagioclase alteration and consequent expansion shatters granitic rock into small fragments (gruss), roughly the size of individual mineral grains (e.g. [11–15]). Grussification is highly dependent on moisture, and therefore on the presence of regolith cover. For example, the importance of cover is strikingly illustrated in Tahoe-aged glacial moraines of the Sierra Nevada, which contain disaggregated granite boulders within their interiors but are mantled with intact boulders of the same lithology on their surfaces [12,13].

Wahrhaftig [12] expanded upon these observations of granite weathering and erosion, and proposed a conceptual model of landscape evolution in granitic terrain in which steep slopes of bare rock and boulders erode much more slowly than gentle footslopes mantled with gruss. In Wahrhaftig's model, bedrock exposed by chance grows first into a tor or small ridge, as surrounding soil-mantled bedrock decomposes to gruss that is washed away by streams. As long as the exposed rock remains steep enough to shed gruss from its slopes, it continues to grow and can eventually form mountainous slopes up to a kilometer in relief. Where bedrock slopes coalesce into ridges, they may control local baselevel and cause the stepped topography that is characteristic of portions of the Sierra Nevada [12].

Wahrhaftig's [12] hypothesis that exposed rock regulates erosion rates and helps generate mountain-scale relief in granitic terrain has remained virtually untested by field measurements. Small et al. [16,17] used cosmogenic nuclides to show that granitic tors erode more slowly than the surrounding terrain, but limited their observations to low-relief summit flats. Here, we examine erosion rates of exposed bedrock and soil-mantled terrain across a wide range of hillslope gradients in granitic mountains of northern California. Our cosmogenic ^{26}Al and ^{10}Be measurements show that erosion rates of boulders and exposed bedrock in the Diamond Mountain batholith are substantially slower than the average erosion rates of the catchments in which they are found. Moreover, boulders and bare rock are much more abundant on steep slopes and may limit erosion rates by protecting deeply weathered saprolite beneath a boulder cover.

2. Site descriptions

The Diamond Mountains are at the transition between the northeastern Sierra Nevada and the Basin and Range, where extension has broken the batholith into a series of fault blocks (Fig. 1). The rainshadow from the Sierran crest to the west produces a semi-arid environment where vegetation ranges from forests of Incense Cedar, Jeffrey Pine and Ponderosa Pine on mountain slopes and ridges, to sagebrush scrub communities in valleys and on low foothills. We focused our sampling in two study areas: one near Adams Peak and another near Antelope Lake (Fig. 1). The Adams Peak study area lies along the west side of the range crest between 2000 m and 2500 m elevation; annual precipitation averages 60 cm/yr [18] and mean annual temperature is 4°C. The Antelope Lake study area is $\sim$35 km northwest of Adams Peak at an elevation of 1700–1800 m. Antelope Lake has a mean annual temperature of 8°C

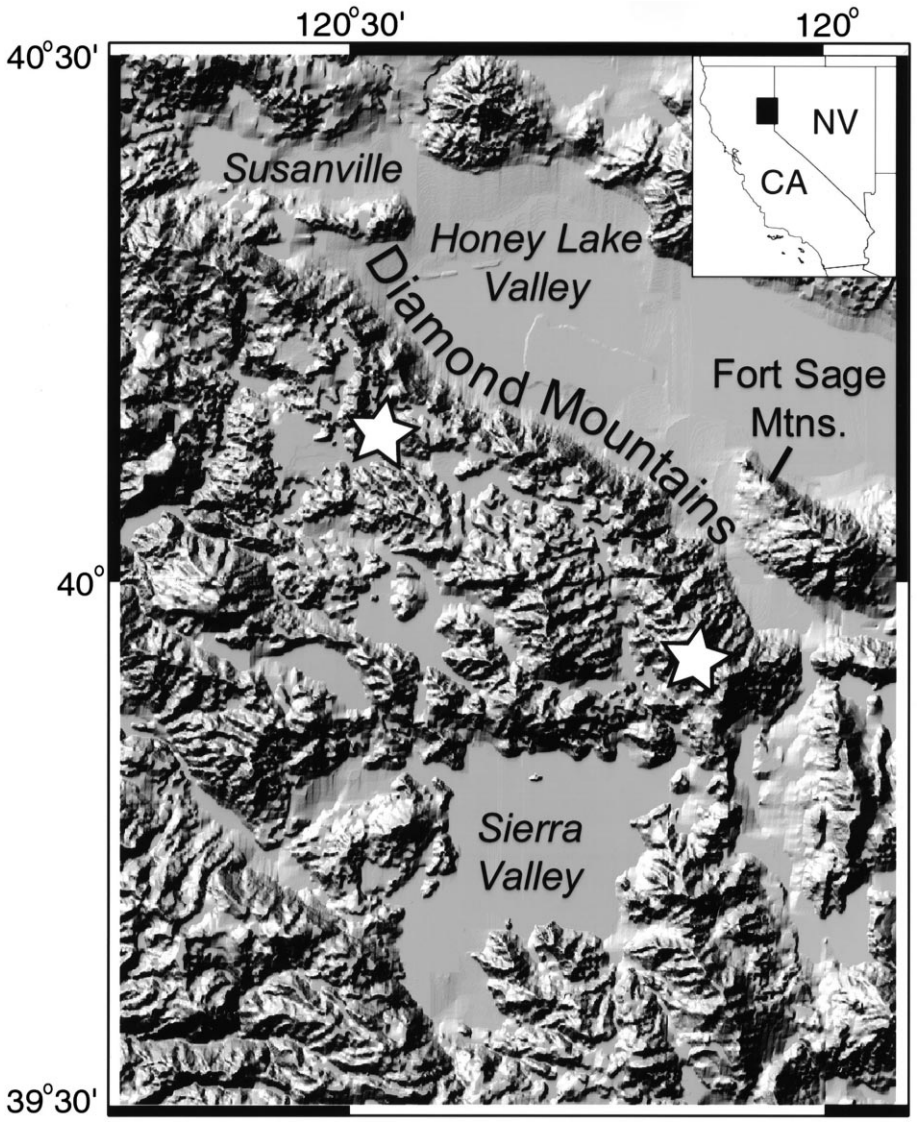

Fig. 1. Shaded relief location map for study sites in the Diamond Mountains, northeastern Sierra Nevada, CA, USA. Stars indicate Adams Peak study area (to the southeast) and Antelope Lake study area (to the northwest). Also shown is the Fort Sage Mountains study area of Granger et al. [42].

and receives more precipitation (90 cm/yr; [18]). Both areas are developed in moderately uniform hornblende-biotite granodiorite and tonalite [19–21] and are far from active faults [21].

The Adams Peak region is characterized by steep ridges and peaks that rise 500 m or more above rolling foothills to the west. The steepest slopes frequently expose jointed bedrock and jumbled boulders; soils on these slopes are thin and primarily limited to valley axes and spaces between boulders. Gentle slopes are primarily soil-mantled, with valley axes containing thick (>1 m) colluvial deposits; soils become thinner towards the ridgetops, where occasional boulders and bare rock crop out. The Antelope Lake region is situated west of the range crest in an area of much lower relief (generally less than 250 m). Knobs and ridges in the area are mantled with

thin soils, with boulders and occasional bedrock exposed on their crests. At both study areas, we selected small (1–100 ha) catchments draining slopes of markedly different steepness but similar lithology and determined their erosion rates using cosmogenic ^{26}Al and ^{10}Be.

3. Measuring erosion rates with cosmogenic ^{26}Al and ^{10}Be

3.1. Theory

Cosmogenic nuclides such as ^{26}Al and ^{10}Be are produced in mineral grains by nuclear reactions with secondary cosmic-ray nucleons and muons [22]. Because cosmic-ray nucleons and muons are rapidly attenuated as they pass through matter, cosmogenic nuclide production is limited to the uppermost several meters of rock near the surface. Production by nucleon spallation decreases roughly exponentially with depth, with a penetration length of 160 ± 10 g/cm^2, or $\sim$60 cm in rock of density 2.6 g/cm^3 [23]. Muons penetrate deeper and continue to produce cosmogenic nuclides at depths opaque to neutrons (e.g. [24]). Recent measurements show that muons produce only 1–3% of ^{26}Al and ^{10}Be in quartz at the surface [24–27]. Nonetheless muon reactions dominate production of these nuclides at depths greater than a few meters and can contribute significantly to the total cosmogenic nuclide inventory measured at the surface [28].

In a steadily eroding rock, the long-term steady-state concentration of ^{26}Al or ^{10}Be (N_i) can be approximated by Eq. 1:

$$N_i(z) = [P_{n,i}/(1/\tau_i + \rho\varepsilon/\Lambda)] + [Y_i A_1/(1/\tau_i + \rho\varepsilon/L_1)] + [Y_i A_2/(1/\tau_i + \rho\varepsilon/L_2)] + [B_i/(1/\tau_i + \rho\varepsilon/L_3)] \quad (1)$$

where the subscript i denotes either ^{26}Al or ^{10}Be, $P_{n,i}$ represents production by nucleon spallation at the surface, τ_i is the radioactive meanlife ($\tau_{26} = 1.02 \pm 0.04$ Myr [29]; $\tau_{10} = 2.18 \pm 0.09$ Myr [30]), ε is the rock's erosion rate, ρ is density, Λ is the penetration length for production by nucleon spallation ($\Lambda = 160 \pm 10$ g/cm^2 [23]), and L_1, L_2, and L_3 are penetration lengths for muon reactions. Y_i is the yield per stopped negative muon, with the stopping rate φ given by [26,28]:

$$\varphi(z) = (A_1 e^{-\rho z/L_1} + A_2 e^{-\rho z/L_2}) \quad (2)$$

Fast muon production scales with depth approximately according to $B_i e^{-\rho z/L_3}$ [24,26]. Eq. 1 is strictly valid only if the rock has been eroding at a constant rate for long enough time (t) to either exhume several penetration lengths, or for radioactive decay to reach steady-state (i.e. $t \gg [1/\tau_i + \rho\varepsilon/\Lambda]^{-1}$; $t \gg [1/\tau_i + \rho\varepsilon/L_1]^{-1}$; $t \gg [1/\tau_i + \rho\varepsilon/L_2]^{-1}$; $t \gg [1/\tau_i + \rho\varepsilon/L_3]^{-1}$).

The production rates and penetration lengths in Eq. 1 must be scaled for latitude and altitude. Production by nucleon spallation may be scaled using table 2 of [31]. Muogenic production should be scaled according to energy. Muons with energy less than $\sim$3 GeV are latitude-dependent due to a changing cosmic-ray cutoff rigidity [32], though to a lesser degree than nucleons. Carmichael and Bercovitch [33] showed that the muon flux is constant below a cutoff rigidity of $\sim$5 GV, compared to $\sim$2 GV for neutrons. In addition, low-energy muons experience losses by radioactive decay in the atmosphere, while muons with energy higher than $\sim$10 GeV travel quickly enough that time dilation by the Lorentz transformation prevents radioactive loss [34]. Altitude scaling therefore depends on muon energy. Muons with energy $\ll$1 GeV should be scaled with an effective attenuation length of 247 g/cm^2 in the atmosphere [34], muons with energies between $\sim$1 GeV and $\sim$10 GeV should be scaled with energy-dependent atmospheric decay rates [35], and higher-energy muons should be adjusted for atmospheric depth following the relationships of Stone et al. [28].

For ^{26}Al and ^{10}Be at sea-level and high latitude, the production constants in Eq. 1 are given by $A_1 = 170.6$ μ^-/g/yr; $A_2 = 36.75$ μ^-/g/yr; $Y_{26} = 4.24 \times 10^{-3}$; $Y_{10} = 5.6 \times 10^{-4}$; $B_{26} = 0.192$ at/g/yr; $B_{10} = 0.026$ at/g/yr; $L_1 = 738.6$ g/cm^2; $L_2 = 2688$ g/cm^2; $L_3 = 4360$ g/cm^2 [26]. At our sites, near a latitude of 40°N, the cosmic-ray cutoff rigidity is

sufficiently low (~4 GV) [36] that muons are unaffected by latitude [33]. Production rates can be scaled for the 2 km altitude of our sites using energy-dependent scaling factors derived from Okuda and Yamamoto [35] (as graphed in [37]) and converting muon energy to depth following Stone et al. [28]. We find that after adjusting the sea-level negative muon stopping rate for atmospheric depth at our sites [28], travel-time corrections must be added to Eq. 2, increasing the muon stopping rate by approximately $\varphi(z) = 280e^{-\rho z/L_4}\mu^-$/g/yr, where $L_4 = 286$ g/cm^2. Though we include such travel-time scaling in our analysis, ignoring this effect does not substantially alter our results.

3.2. The importance of muons

Previous research has generally ignored the role of muons when inferring bedrock erosion rates from ^{26}Al and ^{10}Be (with the exceptions of [25,38]). Eq. 1 shows that ignoring the muon contribution can lead to significant underestimation of the true erosion rate, by approximately 25% in the case of rapidly eroding rock near sea-level at high latitude. Production by muons becomes less important with elevation, because muons are more slowly attenuated in the atmosphere than spallation-producing nucleons. Due to the high elevation and moderate erosion rates (15–60 mm/kyr) of our sites, muons affect our inferred erosion rates by less than 6%. Previous theoretical estimates cited in [39] considered that stopping muons could contribute as much as 16% of the sea-level production of ^{26}Al and ^{10}Be. If this were the case then Eq. 1 suggests that erosion rates at sea-level and high latitude could be underestimated by nearly 50% for quickly eroding sites.

3.3. Sediment mixing

Eq. 1 can be used to determine the steady-state erosion rate of bare rock, but we are interested in determining erosion rates of regolith-mantled catchments where quartz grains in the regolith may have complicated histories of exposure and burial. Several researchers [40–42] have shown that cosmogenic nuclide concentrations in well-mixed sediment can be used to infer the average erosion rate of the sediment's source area, provided that erosion is sufficiently rapid to ignore radioactive decay. Though these earlier analyses did not account for muogenic production, they are easily extended to show that Eq. 1 can be used to infer erosion rates from bulk sediment samples, provided that radioactive decay is negligible (i.e. $\rho\varepsilon/L_3 \gg 1/\tau_i$, or $\varepsilon \gg 16$ m/Myr for ^{26}Al in rock of density 2.6 g/cm^3). If erosion is not fast enough to completely ignore radioactive decay, but is sufficient to ignore decay from nucleon spallation products (i.e. $\varepsilon \gg \Lambda/\rho\tau_i$, or $\varepsilon \gg 0.6$ m/Myr), then Eq. 1 is still valid if soil depth h is much smaller than the effective muon penetration lengths ($h \ll L_1/\rho_{soil} = 4$ m for soil of density 1.8 g/cm^3). If radioactive decay cannot be ignored, then the inferred erosion rate will overestimate the true erosion rate by inadequately representing the most slowly eroding parts of the sediment contributing area.

3.4. The importance of mineral dissolution

As bedrock decomposes to regolith, easily weathered minerals are preferentially dissolved, leaving a quartz-rich residuum. Accurately inferring erosion rates from quartz in the regolith requires consideration of the average residence time of those grains, which is somewhat longer than the average grain in the regolith [17]. The total accumulation of cosmogenic ^{26}Al or ^{10}Be in quartz grains in soil, including the effects of prolonged residence time due to selective enrichment, can be calculated for thin soils ($h \ll 4$ m) as:

$$N_i = [P_n\Lambda/\rho\varepsilon][f_R/f_B + (1-f_R/f_B)e^{-\rho h/\Lambda}] + [Y_i A_1/(1/\tau_i + \rho\varepsilon/L_1)] + [Y_i A_2/(1/\tau_i + \rho\varepsilon/L_2)] + [B_i/(1/\tau_i + \rho\varepsilon/L_3)] \quad (3)$$

where f_R and f_B represent the fraction of quartz in the regolith and bedrock, and h is regolith thickness. We used Eq. 3 to determine catchment erosion rates, substituting f_R and f_B with [Zr] from XRF measurements of regolith and bedrock sam-

ples and accounting for increased production by muons as described in Section 3.1. In our watersheds, quartz and zircon are both effectively insoluble, so zircon enrichment can be used as a proxy for quartz enrichment. Quartz enrichment decreases inferred erosion rates at our sites by a maximum of 12%.

3.5. Bare rock erosion

We also measured bare rock erosion rates at several locations. Determining outcrop erosion rates is not necessarily as simple as measuring [^{26}Al] and [^{10}Be] on the outcrop surface and using Eq. 1. If the outcrop was recently exhumed from beneath a soil cover, then it will have an inherited cosmogenic nuclide profile that depends on the erosion rate of the soil. The steady-state erosion assumption in Eq. 1 is not valid until the outcrop has eroded through several cosmic-ray penetration lengths. We avoided this complication by sampling bedrock only on crags and tors far above any soil cover and used Eq. 1 to calculate erosion rates.

4. Methods

4.1. Cosmogenic nuclide chemistry

We collected bulk sediment samples from streambeds and colluvial hollows and isolated quartz by selectively dissolving other minerals in aqua regia, pyrophosphoric acid, and dilute HF/HNO_3 in an ultrasonic bath (modified from [43,44]). Previous work in a similar environment showed that cosmogenic nuclide concentrations have little dependence on grain size [42]. Nonetheless, bulk samples were separated by grain size, purified to quartz, and recombined in their original mass ratios to eliminate grain size bias. Grains smaller than 0.25 mm were excluded to eliminate wind-blown sediment. Samples were dissolved in HF and HNO_3 and spiked with $\sim$0.7 mg Be. Fluorides were eliminated by repeated fuming in H_2SO_4, and Al and Be were purified by ion chromatography and selective hydroxide precipitation. Al_2O_3 and BeO were prepared for accelerator mass spectrometry (AMS) and mixed with Ag. Measurements were made both at Lawrence Livermore National Laboratory (LLNL) and at PRIME Lab.

4.2. Measuring outcrop abundance and hillslope gradient

We determined the abundance of boulders and bedrock in many of the sampled catchments by stretching a tape measure ($\sim$40 m long) along fall lines at regular intervals, measuring both the fraction of the tape underlain by boulders and bare rock, and average hillslope gradient along the tape.

5. Results and discussion

Catchment erosion rates at Adams Peak and Antelope Lake show similar behavior with varying hillslope gradient (Fig. 2). At gradients below about 0.4, there is a weak correlation between erosion rates and hillslope gradients. More striking is the lack of correlation on steep slopes; for hillslopes with a gradient steeper than 0.45, erosion rates remain constant or even decrease. Catchment-averaged erosion rates remain within a narrow range between 15 and 60 mm/kyr over the entire landscape.

In contrast, bare rock abundance at the two study areas shows a clear relationship with hillslope gradient (Fig. 2). Below gradients of about 0.4, bare rock abundance remains uniformly low. Above a gradient of 0.4, the fraction of boulders and bedrock on the slopes increases rapidly. The steepest slopes are more than half covered with bare rock. The abundance of exposed rock suggests that bare rock erosion may play an important role in this landscape's evolution; it is therefore important to determine bare rock erosion rates. Three samples show that bare rock erosion is significantly slower than catchment averages, at 6–11 mm/kyr (Fig. 2; Table 1).

Because bare rock erodes more slowly than the catchment average, and because exposed bedrock and boulders comprise an increasing fraction of catchments as they become steeper, we suggest

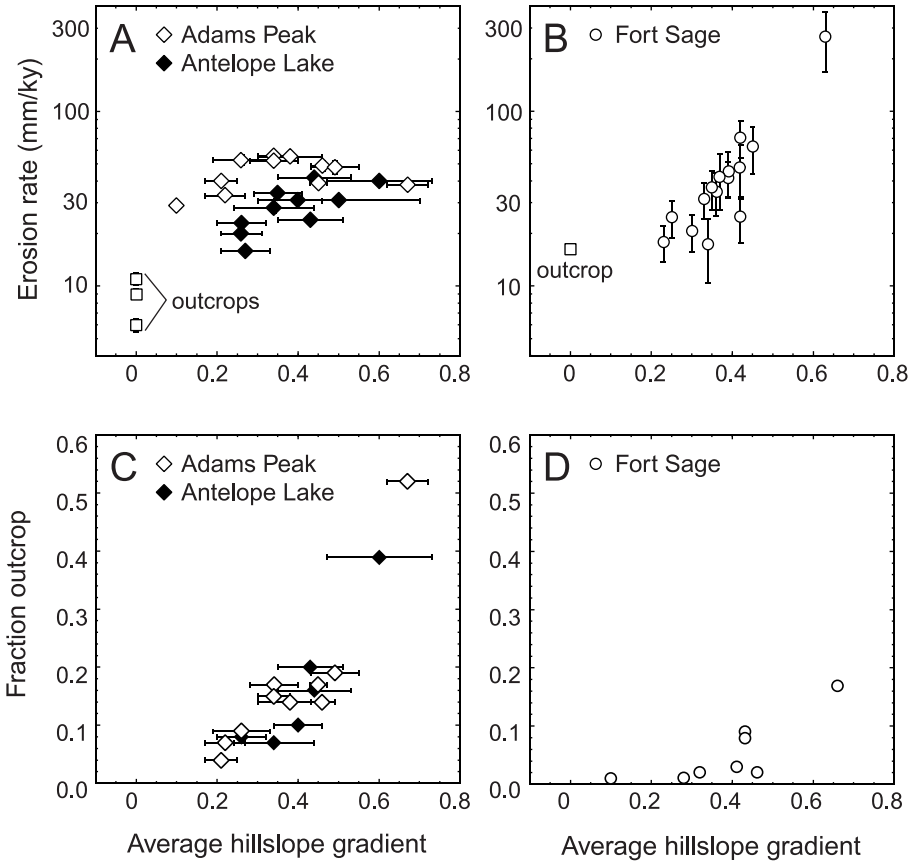

Fig. 2. A and B: Catchment erosion rate plotted against average hillslope gradient (A) for the Diamond Mountains sites, Adams Peak (open diamonds) and Antelope Lake (closed diamonds) and (B) for the Fort Sage Mountain study area (erosion rates are recalculated here using Eq. 3, the data of Granger et al. [42], and additional measurements of soil depth and [Zr]). C and D: Areal fraction of outcrop in catchment plotted against average hillslope gradient (C) for Adams Peak and Antelope Lake and (D) for the Fort Sage Mountain study area.

that bare rock exposure retards erosion of steep slopes and limits the range of erosion rate variability. On steep slopes, prone to rapid sediment transport by rainsplash, sheetwash, and biogenic processes, gruss will be rapidly stripped to expose corestones and bedrock. The exhumed rock will erode much more slowly than the saprolite. Provided that corestones do not roll downhill faster than they are exhumed and that intact bedrock is not exhumed first, a quickly eroding saprolite will accumulate a surface lag of boulders that will shield the underlying saprolite and interrupt rill development during rainstorms (Fig. 3). Saprolite beneath such a boulder cover will continue to weather in place, but grussification and sediment transport will be strongly inhibited by the boulder cover. Exposure of slowly eroding boulders and bedrock provides a negative feedback that can modulate hillslope erosion rates. The faster saprolite is stripped, the more corestones and bedrock will be exhumed to slow the erosion.

Erosion of steep slopes in such a landscape is limited either by the granular disintegration rate of the boulders and bare rock, or by the rate of boulder transport and bedrock landsliding. We see evidence of few bedrock-seated landslides in our study areas, and boulders have not accumulated in valley floors, so boulder erosion appears

Fig. 3. Roadcut near Crystal Peak (~15 km northwest of Adams Peak) showing corestone boulders overlying hand-friable saprolite. These boulders erode slowly and armor underlying saprolite against erosion. Horizontal field of view ~5 m.

to occur primarily by granular disintegration. In contrast, on shallow slopes, transport rates of gruss are sufficiently slow that bedrock is mostly, or entirely, weathered to gruss. Intact rock decays before being exhumed and seldom crops out to retard erosion. Erosion rates on shallow slopes are limited only by the transport rate of gruss. In the Diamond Mountains there appears to be a threshold gradient of approximately 0.45, above which saprolite is stripped and boulders and bare rock modulate erosion.

If boulder armoring inhibits the erosion of steep slopes, then steep granitic slopes should erode rapidly in the absence of boulders. To explore this possibility, we compare erosion rates at the Diamond Mountain study areas with erosion rates in the nearby Fort Sage Mountains [42].

5.1. Comparison with Fort Sage Mountains

The Fort Sage Mountains are a fault block ~20 km east of the Adams Peak study area and are developed in similar bedrock to the Diamond Mountains [20]. The range lies in the rainshadow of the Diamond Mountains at an elevation of 1500 m and receives only 20 cm annual precipitation with a mean annual temperature of 12°C. Vegetation is dominantly sagebrush scrub.

Table 1
Erosion rates inferred from cosmogenic nuclide concentrations in stream sediment and rock outcrops

Sample ID[a]	Elevation (km)	Drainage area (ha)	$[^{10}Be]^b$ (10^5 at/g)	$[^{26}Al]^b$ (10^6 at/g)	$[Zr]^c_{bedrock}$ (ppm)	$[Zr]^c_{regolith}$ (ppm)	Erosion rate $^{10}Be^d$ (mm/kyr)	Erosion rate $^{26}Al^d$ (mm/kyr)	Area bare rock (%)	Average gradient[e] (%)
AP-1	2.05	2.2	4.4 ± 0.1	2.6 ± 0.3	–	–	35 ± 3	35 ± 5	7	22 ± 5
AP-2	2.15	1.1	4.0 ± 0.1	2.3 ± 0.3	–	–	41 ± 3	42 ± 5	17	45 ± 2
AP-3	2.14	3.3	3.0 ± 0.2	2.0 ± 0.2	99 ± 1	122 ± 4	53 ± 5	49 ± 7	14	46 ± 3
AP-4	2.19	1.9	4.1 ± 0.2	2.6 ± 0.3	96 ± 2	104 ± 5	41 ± 4	38 ± 4	52	67 ± 5
AP-5	2.05	7.4	2.5 ± 0.1	1.6 ± 0.2	99 ± 3	115 ± 8	60 ± 7	58 ± 8	15	34 ± 4
AP-6	2.12	13.4	3.1 ± 0.3	–	–	–	51 ± 6	–	19	49 ± 6
AP-7	1.92	1.1	2.4 ± 0.1	1.6 ± 0.2	–	–	59 ± 6	54 ± 7	14	38 ± 3
AP-9	1.94	0.4	2.6 ± 0.1	1.7 ± 0.2	–	–	55 ± 5	52 ± 7	17	34 ± 6
AP-10	2.48	rock	31 ± 2	18 ± 1	–	–	6 ± 1	6 ± 1	–	–
AP-11	2.25	0.4	5.9 ± 0.4	3.0 ± 0.2	96 ± 5	116 ± 5	29 ± 4	37 ± 4	–	10 ± 1
AP-13	1.89	0.4	3.2 ± 0.2	1.8 ± 0.1	96 ± 4	115 ± 2	42 ± 5	46 ± 5	4	21 ± 3
AP-14	1.89	0.7	2.8 ± 0.2	1.5 ± 0.1	–	–	49 ± 5	56 ± 6	9	26 ± 1
AP-15	2.27	rock	–	8.3 ± 0.5	–	–	–	12 ± 1	–	–
AP-16	2.26	rock	19 ± 1	11 ± 1	–	–	8 ± 1	9 ± 1	–	–
AL-2	1.79	3.0	3.5 ± 0.2	2.3 ± 0.1	–	–	38 ± 4	36 ± 4	–	35 ± 6
AL-3	1.74	8.2	3.3 ± 0.2	1.5 ± 0.1	–	–	39 ± 4	50 ± 5	16	42 ± 2
AL-4	1.74	1.9	5.3 ± 0.4	2.9 ± 0.2	172 ± 11	217 ± 17	24 ± 3	27 ± 3	20	43 ± 2
AL-5	1.69	4.5	4.2 ± 0.3	2.4 ± 0.1	155 ± 49	210 ± 11	29 ± 11	30 ± 12	7	34 ± 10
AL-6	1.75	2.6	5.0 ± 0.3	3.3 ± 0.2	–	–	26 ± 3	24 ± 2	8	26 ± 2
AL-7	1.80	3.3	8.2 ± 0.5	4.3 ± 0.2	–	–	16 ± 2	18 ± 2	–	27 ± 6
AL-8	1.76	112	4.2 ± 0.3	2.2 ± 0.1	–	–	31 ± 4	34 ± 5	–	50 ± 20
AL-9	1.80	1.1	3.1 ± 0.2	1.9 ± 0.1	202 ± 25	262 ± 19	42 ± 8	43 ± 7	39	60 ± 13
AL-10	1.80	11.1	4.0 ± 0.3	2.3 ± 0.3	179 ± 2	225 ± 5	33 ± 3	34 ± 3	10	40 ± 6
AL-11	1.73	52	6.2 ± 0.4	3.2 ± 0.2	–	–	20 ± 2	23 ± 2	–	26 ± 5
FS-20	1.50	rock	5.5 ± 0.2	2.6 ± 0.3	–	–	18 ± 1	20 ± 2	–	–

[a]AP, AL and FS designations correspond to samples from the Adams Peak, Antelope Lake and Fort Sage Mountain study areas.

[b]$[^{10}Be]$ and $[^{26}Al]$ calculated from $^{10}Be/^{9}Be$ and $^{26}Al/^{27}Al$ measured by AMS. All samples but FS-20 were measured at LLNL. FS-20 was measured at PRIME Lab. ^{26}Al standards at the two AMS labs agree [50]; ^{10}Be standard at PRIME Lab is derived from NIST 4325 and calibrated to a standard at LLNL prepared by K. Nishiizumi from an ICN solution. Dashes in table indicate no data. Uncertainty is standard error.

[c][Zr] measured by XRF. Reported values are averages for sample localities distributed across the catchment (typical sample size = 12 regolith and three fresh rock outcrop samples per catchment). Uncertainty is standard error.

[d]Erosion rates calculated using Eq. 1 (outcrops) and Eq. 3 (catchments). SLHL spallogenic production rates were scaled to sample altitudes and geographic latitudes (39.83°N for AP and 40.17°N for AL) using Lal's [31] table 2. SL muogenic production rates were scaled to sample elevation accounting for atmospheric depth and adding $280e^{-\rho z/286}\mu^-$/g/yr to the stopping rate to adjust for atmospheric travel-time. Production rates and penetration depths are corrected for geometric and depth shielding [51]. We estimate f_R/f_B (Eq. 3) with $[Zr]_{regolith}/[Zr]_{bedrock}$. For catchments where $[Zr]_{regolith}/[Zr]_{bedrock}$ is unavailable, we use averages of available measurements for each study area (1.19 ± 0.03 for AP catchments and 1.26 ± 0.03 for AL catchments). Soil pits reveal that average soil depth is 37 ± 7 cm for AP and 45 ± 17 cm for AL. Soil density is estimated to be 1.8 ± 0.4 g/cm^3. Uncertainties include $[^{26}Al]$ and $[^{10}Be]$ measurement error, variability in soil depth and density, and uncertainty in quartz enrichment. Uncertainty in cosmogenic nuclide production rates is not included, and would add 10–20% systematic uncertainty to all erosion rates.

[e]Uncertainty represents the standard deviation of multiple measurements from throughout the catchment.

Granger et al. [42] measured concentrations of ^{26}Al and ^{10}Be in sediment from small catchments draining the fault block and showed that erosion rates have a strong dependence on hillslope gradient (Fig. 2), increasing exponentially at gradients up to 0.63. These results lie in stark contrast to the relatively uniform erosion rates of the Diamond Mountains over an even broader range of hillslope gradients, even though the granitic bedrock is similar at the two sites. This disparity may be explained by the lack of boulder armoring at the Fort Sage study area (Fig. 2). Boulder abundance at both of the Fort Sage catchments remains uniformly low, never exceeding 20% even on steep slopes. The Fort Sage Mountains, then, provide a counter proof for the boulder armoring hypothesis by showing that, in the absence of boulder cover, steep slopes erode much more rapidly than gentle slopes.

But why are bare rocks less common at the Fort Sage Mountains sites than at the Diamond Mountains sites? An erosion rate measurement on a 6 m tall tor (FS-20 in Table 1) in the Fort Sage Mountains indicates substantially faster bare rock erosion at this site (17 ± 1 mm/kyr), despite the more arid climate. Bedrock exposed in streambeds and on ridge crests at the Fort Sage sites is often friable by hand, as opposed to harder rock found in similar exposures in the Diamond Mountains. These observations suggest that bedrock in the Fort Sage Mountains may be more easily weathered than in the nearby Diamond Mountains, so corestones are less common and place less of a limit on hillslope erosion. Though the bulk chemistry of the Fort Sage Mountains pluton is similar to the Diamond Mountain batholith [20], differences in other bedrock characteristics such as joint density, grain size, and mineralogy could cause differences in erosion rates. For example, examination of hand specimens reveals that the mafic mineral component of the Fort Sage Mountain bedrock is dominated by biotite, while hornblende is more common in the Diamond Mountain bedrock. This small difference in lithology may account for the difference in bare rock abundance if grussification is largely controlled by biotite hydration. Other work has similarly suggested that small differences in lithology may have large influences on the rate and style of landscape evolution in granitic terrain (e.g. [14]). For example, the topographic contrast between the flat Sherman erosion surface and the steep-sided inselbergs of the southern Laramie Range, WY, USA, has been attributed to small variations in the degree of biotite oxidation in the parent rocks [45].

In light of the Fort Sage results, we suggest that boulders and bare rock in the Diamond Mountains significantly retard erosion of steep slopes. In the absence of boulders and bare rock, granitic slopes weather to gruss and are easily eroded, while the presence of bare rock and boulders inhibits rapid hillslope erosion.

5.2. Implications for persistence of local relief

Differential erosion of bare and covered granite can clearly produce landforms such as tors and bornhardts. However, in our Diamond Mountain study areas where boulders and bare rock cover only a fraction of mountain slopes, their effect on landscape evolution is less extreme. The bare rock serves to slow erosion of steep slopes, bringing the mountain landscape close to a state of dynamic equilibrium [46] in which steep and gentle slopes erode at similar rates. Because erosion is relatively uniform across the landscape, relief reduction will proceed more slowly than it would if steep slopes eroded much faster than their gentle counterparts.

Local relief in the Diamond Mountains appears to be changing very slowly. Our data show that summit erosion is indistinguishable from that of the rest of the landscape. If these erosion rates are representative of the long-term average, then relief can be potentially preserved for millions of years in the absence of fault motion. That relief has been stable over the long term near Adams Peak is supported independently by other geologic evidence; 10 Myr old volcanic flows locally span up to 500 m of elevation [21], indicating that relief in the middle Miocene was, at minimum, over half that of today. Because these 10 Myr volcanic flows still occupy the valley bottom but not the range crest, erosion of the mountain tops has probably reduced local relief somewhat over this time.

Cosmogenic nuclides average erosion rates over roughly the timescale required to erode one neutron penetration length (~60 cm in rock) [31]. Our erosion rates inferred over 10^3–10^4 yr timescales are broadly consistent with exhumation rates averaged over much longer periods of time. House et al. [47] estimate 2–4 km of valley lowering over the past 70–80 Myr from U–Th/He ages in a transect across the central Sierra Nevada, giving long-term lowering rates of 25–60 mm/kyr. These estimates agree remarkably well with our cosmogenic erosion rates of 15–60 mm/kyr.

Our results contrast with estimated rates of relief generation in the nearby Sierra Nevada [16]. Boulders on high (~3.7 km) summit flats in the southern Sierra Nevada near Mount Whitney are eroding at only 2–5 mm/kyr [16], more than a factor of two slower than bare rocks at the Diamond Mountain study areas. These rates are comparable to erosion of glacially scoured bedrock in the same region, where we have observed that erosionally resistant phenocrysts and aplite dikes of the Whitney pluton retain glacial polish and stand 2–5 cm above the surrounding rock after ~13 kyr of postglacial erosion [48]. Small et al. [16] contrasted these slowly eroding summit flats with estimated average erosion rates of 50 mm/kyr and suggested that Sierran relief may be increasing at rates up to 100 m/Myr. The summit flats studied by Small et al. [16] may be remnants of earlier topography that are being consumed by more rapid erosion of the mountain flanks. There is no evidence of broad summit flats near our sites, so such a surface has been completely consumed, if it ever existed.

Erosion rates in our Diamond Mountain sites are comparable to those in the nearby unglaciated Sierra Nevada [49]. Erosion rates are not strongly dependent on hillslope gradient, except in landscapes near rapidly eroding river canyons or fault scarps [49]. This suggests that the processes governing the development of erosional dynamic equilibrium in the Diamond Mountains may be operating throughout the Sierra Nevada. Given the difference in erosion rates between bare and covered rock, Wahrhaftig's [12] hypothesis that slow erosion of bedrock summits and steep slopes generates relief in parts of the Sierra Nevada remains plausible where very steep and gentle slopes are juxtaposed. However, the influence of boulder armoring and local bare rock exposure extends beyond this special situation. At our study areas boulders and bare rock may help maintain relatively uniform erosion rates across the landscape, thereby stabilizing the landscape and reducing the rate of relief generation and decay.

6. Conclusions

It has been widely inferred both from geologic observations (e.g. [1,12,15]) and from previous cosmogenic nuclide measurements [4–6,16,17] that bare rock erodes more slowly than soil-mantled rock. Our cosmogenic measurements from the Diamond Mountain sites show that boulders and bare rock can strongly affect erosion of granitic landscapes. Because corestones are more common on steep slopes, they enforce a negative feedback that slows erosion of steep mountain flanks. Erosion rates are determined by the transport rate of gruss on gentle slopes and by the mechanical breakdown of bare bedrock and boulders or landsliding on steep slopes. Our erosion rate measurements suggest that much of the unglaciated Sierra Nevada may be in erosional dynamic equilibrium, in which steep and gentle slopes lower in concert, maintaining steep mountain flanks and high local relief.

Acknowledgements

This project was supported by NSF Grants EAR-9357931 and EAR-9614442, and was partially performed under the auspices of the US Department of Energy by University of California Lawrence Livermore National Laboratory under contract no. W-7405-Eng-48. We thank N. Brozovic, M. Herzog, and P. McIntyre for field assistance, and A. Granger and J. Gulley for helpful comments on the manuscript. The paper was improved by comments from R. Wieler and an anonymous reviewer, and instructive discussions with J. Stone regarding muons in the atmosphere.*[RV]*

References

[1] G.K. Gilbert, Report on the Geology of the Henry Mountains, US Geographical and Geological Survey, 1877.

[2] N.J. Cox, On the relationship between bedrock lowering and regolith thickness, Earth Surf. Process. Landf. 5 (1980) 271–274.

[3] F. Ahnert, Approaches to dynamic equilibrium in theoretical simulations of slope development, Earth Surf. Process. Landf. 12 (1987) 3–15.

[4] A.M. Heimsath, W.E. Dietrich, K. Nishiizumi, R.C. Finkel, The soil production function and landscape equilibrium, Nature 388 (1997) 358–361.

[5] A.M. Heimsath, W.E. Dietrich, K. Nishiizumi, R.C. Finkel, Cosmogenic nuclides, topography, and the spatial variation of soil depth, Geomorphology 27 (1999) 151–172.

[6] A.M. Heimsath, J. Chappell, W.E. Dietrich, K. Nishiizumi, R.C. Finkel, Soil production on a retreating escarpment in southeastern Australia, Geology 28 (9) (2000) 787–790.

[7] D.L. Linton, The problem of tors, Geograph. J. 121 (1955) 470–487.

[8] C.D. Ollier, The inselbergs of Uganda, Z. Geomorphol. 4 (1960) 43–52.

[9] C.D. Ollier, Some features of granite weathering in Australia, Z. Geomorphol. 9 (1965) 285–304.

[10] M.F. Thomas, The study of inselbergs, Z. Geomorphol. S-B 31 (1978) 1–41.

[11] G.W. Crickmay, Granite pedestal rocks in the southern Appalachian piedmont, J. Geol. 43 (7) (1935) 745–758.

[12] C. Wahrhaftig, Stepped topography of the Southern Sierra Nevada, California, Geol. Soc. Am. Bull. 76 (1965) 1165–1190.

[13] M.M. Clark, Role of biotite in the weathering of igneous rocks as observed in the deposits of Pleistocene glaciers of the Sierra Nevada, California (abstract), Geol. Soc. Am. Spec. Pap. 115 (1968) 36–37.

[14] D. Isherwood, A. Street, Biotite-induced grussification of the Boulder Creek Granodiorite, Boulder County, Colorado, Geol. Soc. Am. Bull. 87 (1976) 366–370.

[15] E.S. Larsen Jr., Batholith and associated rocks of Corona, Elsinore, and San Luis Rey quadrangles southern California, Geological Society of America Memoir 29, 1948, 182 pp.

[16] E.E. Small, R.S. Anderson, J.L. Repka, R. Finkel, Erosion rates of alpine bedrock summit surfaces deduced from in situ ^{10}Be and ^{26}Al, Earth Planet. Sci. Lett. 150 (1997) 413–425.

[17] E. Small, R.S. Anderson, G.S. Hancock, Estimates of the rate of regolith production using ^{10}Be and ^{26}Al from an alpine hillslope, Geomorphology 27 (1999) 131–150.

[18] S.E. Rantz, Mean annual precipitation in the California region, U.S. Geological Survey, 1972.

[19] J.A. Van Couvering, Geology of the Chilcoot Quadrangle, Plumas and Lassen counties, California, M.S., University of California, Los Angeles, CA, 1962.

[20] E.A. Oldenburg, Chemical and petrologic comparison of Cretaceous plutonic rocks from the Diamond Mountains, Fort Sage Mountains, and Yuba Pass region of northeastern California, M.S., Humboldt State University, 1995.

[21] T.L.T. Grose, M. Mergner, Geologic map of the Chilcoot 15 minute quadrangle, California, California Division of Mines and Geology, in press.

[22] D. Lal, B. Peters, Cosmic ray produced radioactivity on the Earth, in: S. Flugge (Ed.), Handbuch der Physik 46, Springer-Verlag, Berlin, 1967, pp. 551–612.

[23] J. Masarik, R.C. Reedy, Terrestrial cosmogenic-nuclide production systematics calculated from numerical simulations, Earth Planet. Sci. Lett. 136 (1995) 381–395.

[24] B.P. Heisinger, Myonen-induzierte produktion von radionukliden, Ph.D., Technischen Universität Munchen, 1998.

[25] E.T. Brown, D.L. Bourles, F. Colin, G.M. Raisbeck, F. Yiou, S. Desgarceaux, Evidence for muon-induced in situ production of ^{10}Be in near-surface rocks from the Congo, Geophys. Res. Lett. 22 (6) (1995) 703–706.

[26] D.E. Granger, A.L. Smith, Dating buried sediments using radioactive decay and muogenic production of ^{26}Al and ^{10}Be, Nucl. Instrum. Methods Phys. Res. B 172 (1–4) (2000) 824–828.

[27] B. Heisinger, M. Niedermayer, F.J. Hartmann, G. Korschinek, E. Nolte, G. Morteani, S. Neumaier, C. Petitjean, P. Kubik, A. Synal, S. Ivy-Ochs, In-situ production of radionuclides at great depths, Nucl. Instrum. Methods Phys. Res. B 123 (1997) 341–346.

[28] J.O.H. Stone, J.M. Evans, L.K. Fifield, G.L. Allan, R.G. Cresswell, Cosmogenic chlorine-36 production in calcite by muons, Geochim. Cosmochim. Acta 62 (3) (1998) 433–454.

[29] T.L. Norris, A.J. Gancarz, D.J. Rokop, K.W. Thomas, Half-life of ^{26}Al, Proceedings of the Fourteenth Lunar and Planetary Science Conference, Part I, J. Geophys. Res. 88 (1983) B331–B333.

[30] R. Middleton, L. Brown, B. Dezfouly-Arjomandy, J. Klein, On ^{10}Be standards and the half-life of ^{10}Be, Nucl. Instrum. Methods Phys. Res. B 82 (1993) 399–403.

[31] D. Lal, Cosmic ray labeling of erosion surfaces: in situ nuclide production rates and erosion models, Earth Planet. Sci. Lett. 104 (1991) 424–439.

[32] O.C. Allkofer, H. Jokisch, A survey of the recent measurements of the absolute vertical cosmic-ray muon flux at sea level, Il Nuovo Cimento 15A (3) (1973) 371–389.

[33] H. Carmichael, M. Bercovitch, V. Analysis of IQSY cosmic-ray survey measurements, Can. J. Phys. 47 (1969) 2073–2093.

[34] B. Rossi, Interpretation of cosmic-ray phenomena, Rev. Mod. Phys. 20 (3) (1948) 537–583.

[35] H. Okuda, Y. Yamamoto, Cosmic rays in the upper atmosphere, Rep. Ionos. Space Phys. 19 (1965) 322.

[36] M.A. Shea, D.F. Smart, L.C. Gentile, Estimating cosmic ray vertical cutoff rigidities as a function of the McIlwain L-Parameter for different epochs of the geomagnetic field, Phys. Earth Planet. Inter. 48 (1987) 200–205.

[37] S. Hayakawa, Cosmic Ray Physics: Nuclear and Astro-

physical Aspects, John Wiley and Sons, New York, 1969, 774 pp.
[38] W. Hampel, J. Tagaki, K. Sakamoto, S. Tanaka, Measurement of muon-induced ^{26}Al in terrestrial silicate rock, J. Geophys. Res. 80 (26) (1975) 3757–3760.
[39] K. Nishiizumi, E.L. Winterer, C.P. Kohl, J. Klein, R. Middleton, D. Lal, J.R. Arnold, Cosmic ray production rates of ^{10}Be and ^{26}Al in quartz from glacially polished rocks, J. Geophys. Res. 94 (B12) (1989) 17907–17915.
[40] E.T. Brown, R.F. Stallard, M.C. Larsen, G.M. Raisbeck, F. Yiou, Denudation rates determined from the accumulation of in situ-produced ^{10}Be in the Luquillo Experimental Forest, Puerto Rico, Earth Planet. Sci. Lett. 129 (1995) 193–202.
[41] P.R. Bierman, E.J. Steig, Estimating rates of denudation using cosmogenic isotope abundances in sediment, Earth Surf. Process. Landf. 21 (1996) 125–139.
[42] D.E. Granger, J.W. Kirchner, R. Finkel, Spatially averaged long-term erosion rates from in-situ produced cosmogenic nuclides in alluvial sediment, J. Geol. 104 (1996) 249–257.
[43] C.P. Kohl, K. Nishiizumi, Chemical isolation of quartz for measurement of in-situ-produced cosmogenic nuclides, Geochim. Cosmochim. Acta 56 (1992) 3583–3587.
[44] D.E. Granger, Landscape erosion and river downcutting rates from cosmogenic nuclides in sediment, Ph.D., University of California, Berkeley, 1996.
[45] D.H. Eggler, E.E. Larson, W.C. Bradley, Granites, grusses, and the Sherman erosion surface, southern Laramie Range, Colorado-Wyoming, Am. J. Sci. 267 (1969) 510–522.
[46] J.T. Hack, Interpretation of erosional topography in humid temperate regions, Am. J. Sci. 258-A (1960) 80–97.
[47] M.A. House, B.P. Wernicke, K.A. Farley, Dating topography of the Sierra Nevada, California, using apatite (U–Th)/He ages, Nature 396 (1998) 66–69.
[48] D.H. Clark, P.R. Bierman, P. Larsen, Improving in situ cosmogenic chronometers, Quat. Res. 44 (1995) 367–377.
[49] C.S. Riebe, J.W. Kirchner, D.E. Granger, R.C. Finkel, Erosional equilibrium and disequilibrium in the Sierra Nevada mountains, inferred from cosmogenic ^{26}Al and ^{10}Be in alluvial sediment, Geology 28 (9) (2000) 803–806.
[50] S. Vogt, M.-S. Wang, R. Li, M. Lipschutz, Chemistry operations at Purdue's accelerator mass spectrometry facility, Nucl. Instr. Methods Phys. Res. B 92 (1994) 153–157.
[51] A. Dunne, D. Elmore, P. Muzikar, Scaling of cosmogenic nuclide production rates for geometric shielding and attenuation at depth on sloped surfaces, Geomorphology 27 (1–2) (1999) 3–11.